Available online at www.sciencedirect.com
SCIENCE DIRECT®
Journal of Electroanalytical Chemistry 554–555 (2003) 417–425
Journal of Electroanalytical Chemistry
www.elsevier.com/locate/jelechem

Adsorption and photon-driven charge transfer of pyridine on a cobalt electrode analyzed by surface enhanced Raman spectroscopy and relevant theories

Y. Xie [1], D.Y. Wu, G.K. Liu, Z.F. Huang, B. Ren, J.W. Yan, Z.L. Yang, Z.Q. Tian *

State Key Laboratory for Physical Chemistry of Solid Surfaces and Department of Chemistry, Xiamen University, Xiamen 361005, China

Received 2 January 2003; received in revised form 19 March 2003; accepted 6 April 2003

In memory of Michael Weaver

Abstract

Surface enhanced Raman spectroscopy (SERS) has been applied to study the interaction of pyridine with a cobalt electrode surface. A set of good quality SERS spectra was obtained by using an appropriate surface-roughening procedure and a highly sensitive confocal Raman microscope. The surface enhancement factor was about three orders of magnitude calculated from experimental data and analyzed by the relevant theories. The electromagnetic contribution accounts for two out of the three orders of magnitude mainly through the lightning-rod effect. The remaining enhancement originates from the photon-driven charge transfer mechanism. The SERS intensity-potential profile shows the existence of two charge transfer processes. One is the excitation of the metal 4s orbital to the mixing orbital of the metal $4p_x$ and π-type $3b_1$ of pyridine, and the other is from the metal 3d orbital to the π-type $2a_2$ orbital of pyridine. Furthermore, the spectral difference for the adsorbed pyridine on cobalt and silver surfaces indicates that the chemical interaction of pyridine with the former is considerably stronger than the latter.

Keywords: Surface enhanced Raman spectroscopy; Cobalt electrode; Pyridine; Adsorption; SERS mechanism

1. Introduction

As one of the most important transition metals, cobalt (Co) and its compounds have been widely used in many technological applications including electrochemistry [1–3]. In order to have a thorough knowledge of the properties of the metal, including its related processes and mechanisms, a wide variety of spectroscopic techniques have been employed to study the processes and reactions on Co electrodes [4–10]. Compared with the conventional electrochemical techniques, these techniques have some advantages in monitoring in situ the surface and interfacial processes at the molecular/atomic level. Surface enhanced Raman spectroscopy (SERS), with its very high surface sensitivity and selectivity, can detect the surface species and minimize the interference from the bulk [11–16]. As an in situ diagnostic probe, SERS also has the capacity to provide bonding information between adsorbed molecule and substrate. It has been applied to a variety of surface systems, including electrochemical, biological and other ambient interfaces [17–19]. The fact that only Ag, Au and Cu produce the largest surface enhancements severely limits the use of other metallic materials as the SERS substrate. Extending the range of SERS applications to other metallic and non-metallic surfaces has been a long-term issue in the communities of surface science and spectroscopy [20–31].

In order to extend SERS to Co and other materials, a strategy based on 'borrowing SERS' was proposed and developed by both the Weaver and Fleischmann groups independently [24,25]. This concept was realized by

* Corresponding author. Tel.: +86-592-218-1906; fax: +86-592-218-3047.
E-mail address: zqtian@xmu.edu.cn (Z.Q. Tian).
[1] Present address: Department of Chemistry, Purdue University, West Lafayette, IN, 47907-1393 USA.

0022-0728/03/$ - see front matter © 2003 Elsevier B.V. All rights reserved.
doi:10.1016/S0022-0728(03)00318-8

depositing an ultra-thin Co film over the highly SERS-active Ag substrate [25]. With the aid of the long-range effect of the electromagnetic (EM) enhancement created by the SERS-active substrate underneath, weak SERS spectra of adsorbate on the transition metal over-layer can be obtained. Since the strong EM field generated on the SERS-active substrate is damped significantly by the coated film, the film must be ultra-thin, normally only several atomic layers. Originally, it was very difficult to cover the rough substrate completely with such a thin film. In the mid-1990s, Weaver and coworkers made significant progress in solving this problem. They reported a series of work on 'pinhole-free' transition metal layers over the SERS-active Au surface, which was accomplished by electrochemical atomic-layer epitaxial growth using constant-current deposition at a low current density [32–34] or by redox replacement of under-potential-deposited metals on Au [35]. It has been shown that this method is very promising if one can prepare the 'pinhole-free' ultra-thin film for different materials with good stability in a wide range of potentials and/or temperatures. In addition to studying surface adsorption and reaction, the over-layer method has been used to characterize the fine structure of the ultra-thin film itself. This includes oxides [27], semiconductors [36] and polymers [37]. It makes SERS a versatile tool for studying various material surfaces of practical importance.

Another strategy, not involving 'borrowing', is to generate SERS directly from the massive Co metal, since the ultra-thin Co films may have different crystalline structures and other chemical and physical properties compared to the Co bulk phase commonly formed by metallurgy. However, this strategy is much more challenging as it contradicts the widely accepted notion that transition metals are not SERS-active. Since the early days of SERS, several groups have attempted to obtain SERS signals from adsorbates on roughened Pt and Rh electrodes [28,29], or porous Ni, Pd, Pt, Ti and Co films [23]. However, surface Raman signals from these studies were typically too weak to be investigated as a function of the electrode potential or temperature, some results could even not be repeated by other groups. The results were not strongly supportive of SERS studies on transition metals, and pointed to a gloomy future in this direction. Recently, with the aid of new generation Raman instruments with high sensitivity and the development of surface-roughening procedures, high-quality SERS signal has been obtained from a series of massive transition metals such as Pt, Fe, Ni and Rh [38–44]. Very recently, we reported a study of SERS from bare Co electrodes [45]. Here, we present a systematic study of SERS and the relevant theoretical calculations on the interaction of pyridine with Co electrode surfaces.

2. Experimental

Raman spectra were obtained using two confocal microprobe Raman Instruments: LabRam I (Dilor) and R1000 (Renishaw). The excitation wavelength of 632.8 nm (LabRam I) was used from an internal He–Ne laser with a power of 3 mW at the electrode surface; the 514.5 nm (R1000) was from an external Ar-ion laser with a power of 5 mW at the surface.

Various surface-roughening procedures were employed, which will be described in the following sections. Prior to the surface pretreatment, the Co electrode with a diameter of about 2 mm was first mechanically polished with 0.3 and 0.05 μm alumina powder to a mirror finish followed by ultrasonic cleaning in Milli-Q water. Then, the electrode was subjected to a specific roughening treatment followed by a thorough rinsing with Milli-Q water and finally transferred to the spectroelectrochemical cell for measurement. A large platinum ring served as the counter electrode. A detailed description of the spectroelectrochemical measurement has been given elsewhere [46]. Atomic force microscopy (AFM) images of roughened Co surfaces were recorded on the SPM system (NT-MDT, Solver). All the potentials were quoted versus the saturated calomel electrode. All the chemicals were analytical grade reagents and the solutions were prepared using Milli-Q water.

A model of a prolate hemispheroid of cobalt metal protruding on a flat plane without taking into account the coupling between particles has been used to calculate the local optical electric field contributing to the SERS. The calculation of the chemical enhancement and charge transfer from Co to pyridine is based on density functional theory at the level of B3LYP/6-311+G** (for C, N, H)/LanL2DZ (for metals). A detailed description has been given elsewhere [46].

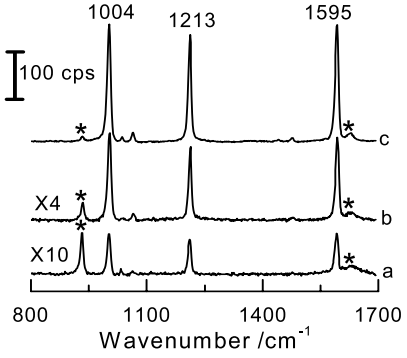

Fig. 1. The SERS spectra of Py obtained at −1.2 V on cobalt electrodes in 10^{-2} M Py+0.1 M $NaClO_4$ with different treatment: (a) chemical etching; (b) ex situ orc; (c) in situ orc. The laser excitation line was 632.8 nm. The peaks marked with asterisks are from the solution.

3. Results and discussion

Fig. 1 illustrates the impact of different surface-roughening procedures on the surface Raman intensity of pyridine adsorbed on Co electrode surfaces. The peaks marked with asterisks are from the solution. After being well polished and cleaned with triply distilled water, the Co electrode was chemically etched in 1 M HNO_3 in the sonication bath for 10 min. As can been seen in Fig. 1a, the surface Raman signal is quite weak; the signal for the strongest band (ν_1, ring-breathing mode) of pyridine is only about 15 counts per second (cps). In order to obtain a stronger signal, the chemically etched Co electrode was subjected to a further electrochemical post-treatment. By applying a double-step oxidation–reduction cycle (orc) ex situ in 0.1 M KCl free of pyridine from -0.4 to $+0.4$ V for 3 s and then back to -0.4 V, a surface Raman signal as strong as 45 cps can be obtained (Fig. 1b). This is about three times stronger in intensity compared with that from the chemically etched Co surface. More surprisingly, if the Co electrode was further treated in 0.1 M KCl with 0.01 M pyridine in situ in the spectroelectrochemical cell using the same roughening procedure, a surface Raman signal of the adsorbed pyridine as strong as 250 cps can be obtained (Fig. 1c). This comparative experiment clearly indicates that, in order to obtain reasonably good spectra for detailed investigations, the proper surface-roughening procedure is necessary.

Through the systematical study on the roughening method, it was found that a combination of chemical etching (in 1 M HNO_3) and electrochemical roughening on the mechanically polished Co electrode provided the best results. A Co electrode with reasonably high surface enhancement, good stability and uniformity can be obtained reproducibly. The detailed roughening procedure is as follows: a mirror finish Co electrode is chemically etched in the HNO_3 solution for 20 s followed by a cathodic polarization in a 0.1 M $NaClO_4$ solution at -1.4 V for hydrogen evolution to expel possible contaminants. Then the potential is stepped to -1.2 V and held for 20 s. After that, the potential is scanned to 1.0 V at a rate of 200 mV s^{-1} and returned to -1.25 V at a rate of 100 mV s^{-1}. Finally, the electrode is kept at -1.25 V for 150 s to reduce the cobalt oxide at the surface completely. Cleaned with Milli-Q water, the cobalt electrode is immersed in a solution of 0.1 M $NaClO_4$ + 0.01 M Py at open circuit potential for further in situ Raman experiments.

The surface, after being chemically etched, and the same surface after further electrochemical roughening were characterized by AFM. Fig. 2 shows that the chemically etched surface is rather uneven, with some bumps of around 200 nm in diameter, while the surface roughened by orcs involves bumps about 2–5 μm over the whole surface. On each bump, the AFM image can clearly identify the presence of cauliflower-like structures with fine particles around 150–300 nm. It is of interest that this structure is similar to that obtained from other transition metals, such as Ni, Fe and Rh, with optimized surface Raman signals.

The higher quality surface Raman signal obtained from the Co surface enables us to investigate the adsorption behavior of pyridine in detail. The potential-dependent surface Raman spectra are shown in Fig. 3. The assignment of the main Raman bands of pyridine in the solution and at the Co surface is listed in Table 1. At a relatively positive potential such as -0.8 V, the Raman intensity is very weak, so the Raman spectrum at this potential was used as the reference. By subtracting each spectrum recorded at different potentials from the spectrum of -0.8 V, one can remove the interference of the bulk solution signal from not only ClO_4^- but also from water and obtain a set of potential-dependent spectra. As can be seen in Fig. 3, the Raman signal increases sharply in intensity as the potential moves negatively, and reaches its maximum at about -1.08 V. The signal decreases quickly at -1.30 V, due to the occurrence of hydrogen evolution at the surface. When the potential was reversed from -1.30 to -0.8 V, the surface Raman signal recovered with a slight decrease in the intensity. The reversibility of this kind of roughened cobalt electrode is reasonably good compared with that of silver and copper electrodes [48].

All surface Raman bands are also changed in frequency with the potential. They are red-shifted about 3–5 cm^{-1} with $d\nu/dE = 10$–17 cm^{-1} V^{-1} as the potential is moved from -0.9 to -1.2 V. This phenomenon is frequently termed the electrochemical Stark effect. These frequency-potential dependences originate from potential-dependent metal-adsorbate bonding and from the influence of the variable electronic field exerted across the adsorbed layer. In the present case, Py can interact strongly with the Co surface so the applied potential could influence the Py intermolecular bond and the metal–Py bond considerably. Evidence supporting this assumption is provided from the low wave-number region. A broad band at around 220 cm^{-1} can be observed in the entire potential range studied (Fig. 3), which is assigned to the Co–N vibration. At relatively negative potentials, a peak at around 232 cm^{-1} emerged from this broad feature. This may infer the increase of the chemical interaction between adsorbed molecule and cobalt surface. The presence of this broad band also indicates that the pyridine molecule is adsorbed at the surface taking the end-on bonding configuration through the nitrogen atom. Furthermore, it suggests that the roughened surface offers different chemical surroundings for adsorbed molecules. When pyridine molecules adsorb at different positions, the force constant of the Co–N band may be altered. Nevertheless, the Co–Co band may

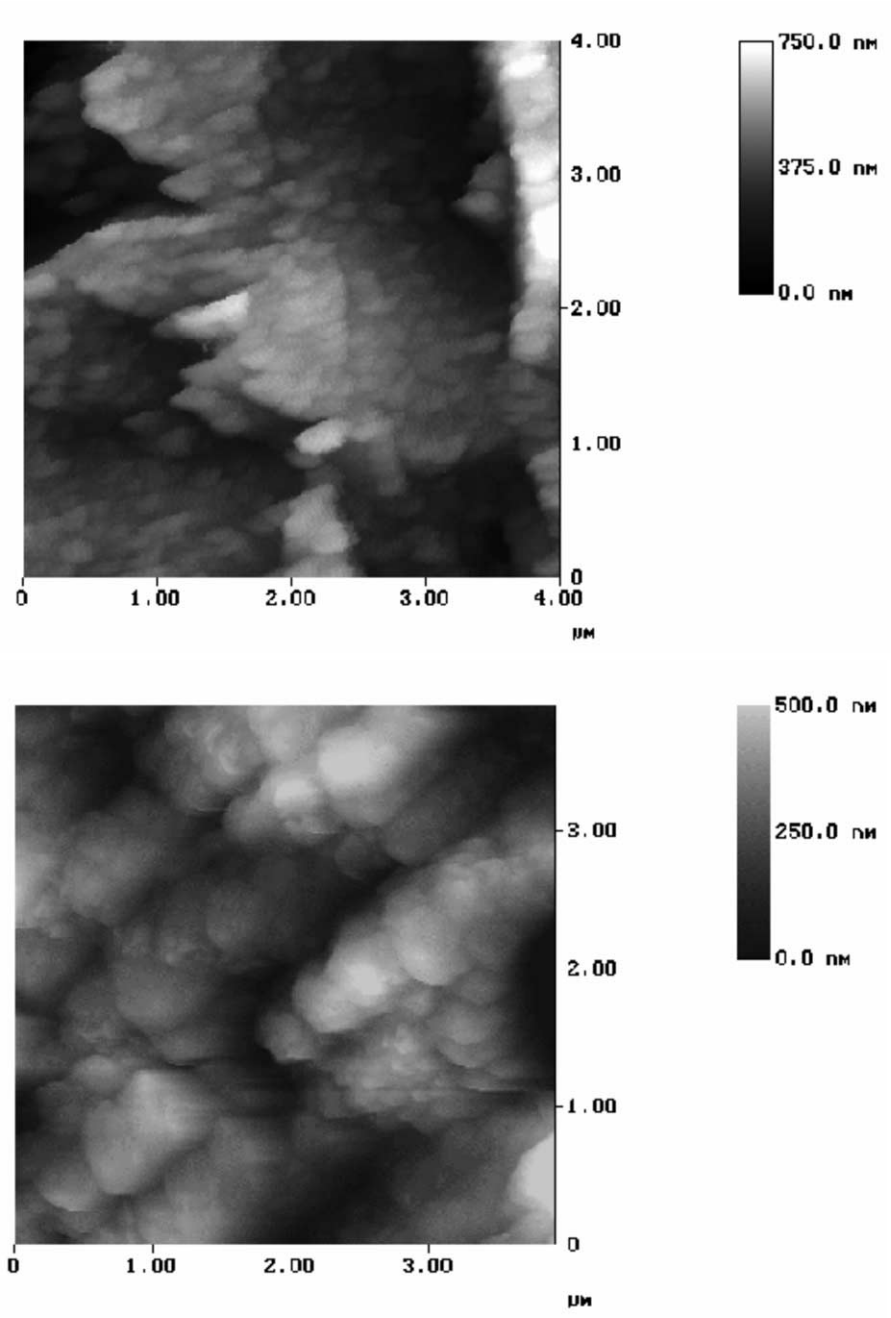

Fig. 2. The AFM images of Co surfaces roughened by (a) chemical etching and (b) the chemical etching combined with electrochemical oxidation and reduction cycling (orc).

partially contribute to this abnormally broad band. Although the vibrational frequency of the cobalt dimer is about 297 cm^{-1}, the vibrational frequency of the Co–Co band should be lower for the large cobalt clusters on rough surfaces owing to the weak metal bonding with respect to that in the cobalt dimer [49]. It should also be noted that surface Raman spectra obtained in the low wave-number region could be used to verify easily if the electrode surface is formed with the oxide film, as several bands from various cobalt oxides are located in the region from 450 to 700 cm^{-1}.

As can be seen from Fig. 3 and Table 1, the bands from in-plane vibration modes are completely dominant in the surface Raman spectra. According to the surface selection rules [14], the pyridine molecule could be considered to adsorb perpendicular or tilted to the cobalt surface. It is necessary to notice the significant changes in the relative intensity of the 1005 (ν_1, ring-breathing), 1214 (ν_{9a}, C–H deformation), 1595 cm^{-1} (ν_{8a}, ring stretching) bands, as shown in Fig. 3. Their potential-dependent relative intensities are clearly shown in Fig. 4. The intensity ratio of the latter two

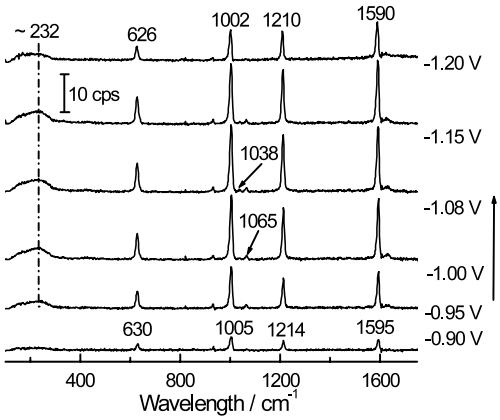

Fig. 3. The potential-dependent SERS spectra of Py adsorption on the cobalt electrode in 10^{-2} M Py+0.1 M $NaClO_4$. The laser excitation line was 632.8 nm.

Table 1
The assignment of frequencies of pyridine absorbed on cobalt and in aqueous solution

Frequencies/ cm^{-1}		Symmetry class (C_{2v})	Assignment
SERS	Solution		
~ 220			N–Co bond stretching
630	616	a_1	ν_{6a} (in-plane ring deformation)
1005	1003	a_1	ν_1 (ring-breathing)
1038	1036	a_1	ν_{12} (trigonal ring-breathing)
1065	1070	a_1	ν_{18a} (in-plane C–H bending)
1214	1218	a_1	ν_{9a} (in-plane C–H bending)
1595	1595	a_1	ν_{8a} (ring stretching)

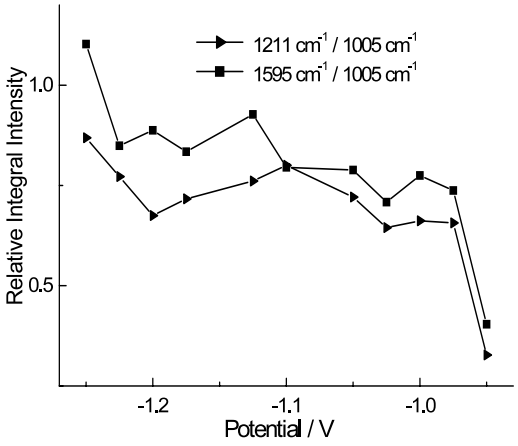

Fig. 4. The profiles of the integral intensity of different vibration bands of adsorbed Py as a function of the potential in 10^{-2} M Py+0.1 M $NaClO_4$. The laser excitation line was 632.8 nm.

bands to the first one increase from 0.3 and 0.4 at −0.95 V to 0.9 and 1.1 at −1.25 V, respectively. This behavior is more profound than that observed from other metals, such as Ag, Au, Cu and Pt [14,43,46]. It may imply a considerable interaction between the adsorbate and substrate. Besides the features of the electrode surface, another important factor contributing to the potential-dependent spectral features is the SERS mechanism.

Before discussing the possible SERS mechanism, it is necessary first to ensure that the roughened cobalt electrode exhibits SERS activity. Taking the spectrum obtained at −1.08 V shown in Fig. 3, we calculated the enhancement factor (EF) specific to our confocal Raman system [41]. The factor G is about 1.03×10^3, indicating that there are about three orders of amplification for the surface Raman signal. Therefore, to understand the enhancement mechanism for cobalt surfaces, two theoretical calculations based on the EM field enhancement [16] and the charge transfer (CT) enhancement [15], respectively, were carried out.

The EM field enhancement is one of the two most important aspects of SERS [14–16]. The EM field at the surface can be greatly enhanced due to surface plasmon resonance, especially for the noble metals. However, for the transition metals including cobalt, generally speaking, the Fermi level locates within the range of d-bands and the interband electron transition can be excited by visible light, so the surface plasmon resonance is not as effective as that in noble metals. Nevertheless, we calculated a simple model of a prolate hemispheroid of cobalt metal protruding on a flat plane based on the previous theoretical calculation for the noble metal [47,50]. Thus the EM field EF can be expressed by [47]

$$EF = \frac{L(\omega_i)^2}{|1 - \Gamma(\omega_i)|^2} \frac{L(\omega_s)^2}{|1 - \Gamma(\omega_s)|^2} \tag{1}$$

where the image field effect $\Gamma(\omega)$ and the shape effect $L(\omega)$ in the above equation are given as

$$\Gamma(\omega) = \frac{\alpha}{4(f\xi_1)^3} + \frac{2\alpha[\varepsilon(\omega) - 1]}{f^3} \times \sum_n{}' \frac{(2n+1)P_n(\xi_0)P_n'(\xi_0)[Q_n'(\xi_1)]^2}{\varepsilon(\omega)P_n'(\xi_0)Q_n(\xi_0) - P_n(\xi_0)Q_n'(\xi_0)} \tag{2}$$

$$L(\omega) = \left| \frac{1 - \varepsilon(\omega)}{\varepsilon(\omega)Q_1(\xi_0) - \xi_0 Q_1'(\xi_0)} \right| \tag{3}$$

where $P_n(\xi)$ and $P_n'(\xi)$ are the first kind nth order Legendre function and its derivatives, $Q_n(\xi)$ and $Q_n'(\xi)$ are the second kind nth order Legendre function and its derivatives, f and ξ are the focus distance and the radial coordinate in the spheroid coordinate system, respectively. α is the polarizability of the adsorbed molecule. The prime at the top right corner of the sum symbol indicates that only odd n terms appear in the summation. ω_i and ω_s are frequencies of the excitation and scattering lights, and have a relation of $\omega_s = \omega_i - \omega_v$, in which ω_v is the vibrational frequency of a given normal mode. In our calculation, $\varepsilon(\omega)$, denotes the dielectric constant, depending on the excitation frequency of the

incident and scattered lights and the optical properties of the materials. The EF we calculated was for a vibrational mode with the dipole moment changes along the z-axis. When the optical dielectric constants of the ambient medium of 1.0 for vacuum and 1.77 for water were adopted, the changes in the EM EF with the aspect ratio and size as well as the exciting photon energies are shown in Fig. 5. The calculated result shows that the SERS signal depends on the shape and the size of the prolate and the ambient medium. A comparison of the EM EFs in Fig. 5a and b indicates that the medium effect results in the shift of the maximum of the EM enhancement to the low-energy side. However, the largest EM EF remains almost unchanged. In contrast to the enhancement effect of the noble metal [51,52], the curves obtained from cobalt are much broader, as seen in Fig. 5. This infers that the enhancement does not depend critically on the excitation line. Since the most efficient enhancement occurs along the semimajor axis of the prolate spheroid, a factor of $\sim 1/17$ for scaling the top enhancement was used to obtain the average effect for the whole nanoparticle. The average EM EF of $\sim$ 100-fold is reasonable at the excitation lines of 514.5 and 632.8 nm to interpret the EM mechanism of the roughened Co electrode. This value is similar to that obtained from the electrodynamics calculation on spheroids of Pt, Rh, Ni and Pd by Chang and coworkers [53,54]. In our previous experiment on transition metal nanowire arrays, it was found that the SERS activity increased remarkably with the increase of the wire length [55]. The experimental data and theoretical calculation both indicate that the lightning-rod effect plays an important role in the EM enhancement for cobalt.

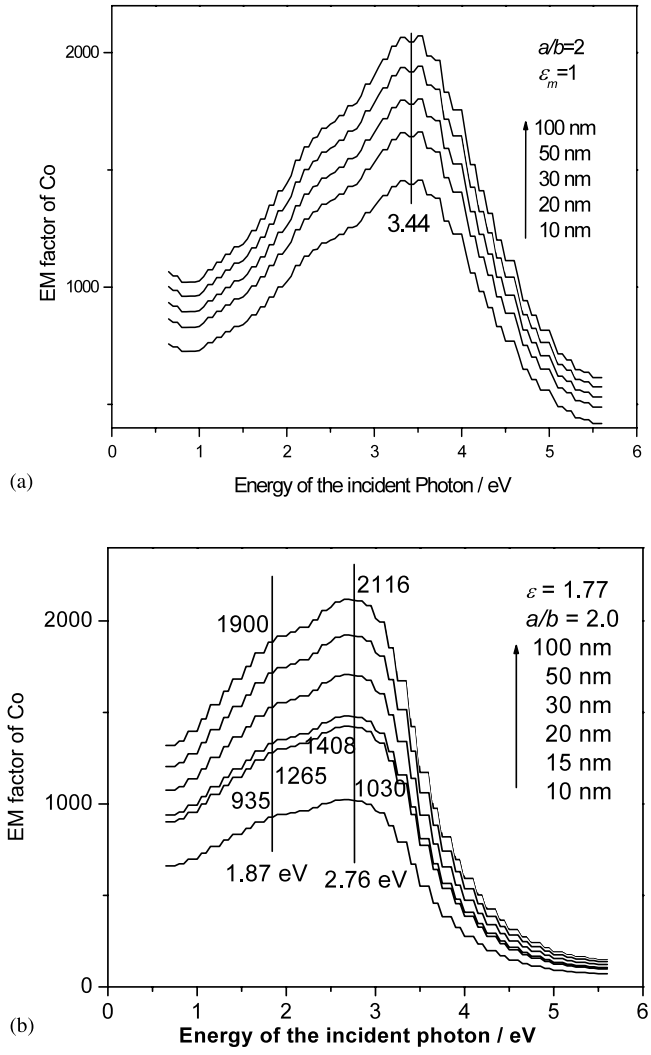

Fig. 5. Changes of the EM EFs by evaluating a polarized dipole located at the tip of a hemispheroid with an aspect ratio, $a/b = 2$, on a conduction plane. (a) Vacuum $\varepsilon_m = 1.0$ and (b) water $\varepsilon_m = 1.77$. This dipole system is the ring-breathing mode of pyridine, which has a vibrational frequency of 1008 cm^{-1}.

Compared to the contribution to the EM enhancement from the interaction of the incident photons and the metal, the CT enhancement is associated with the chemical interaction of the metal and the adsorbate, which can be explained by a resonance-like Raman mechanism [15,56–58]. As the Py/Co system involves the formation of chemical bonds for the adsorbate with the electrode surface, it is necessary to discuss the CT enhancement in more detail. The photon-driven CT enhancement, in fact, can be easily verified by obtaining the intensity-potential profile with the changing exciting line (i.e. changing the incident photon energy) [15,46,56–58]. Fig. 6 shows two profiles of the SERS intensity of the ν_1 mode of pyridine as the potential is changed. As the exciting line changes from 514.5 to 632.8 nm, the peak potential moves to a more negative potential. The difference in the peak potential of the two profiles is about 100 mV. This means that, with an increase of the wavelength of the incident laser, the peak

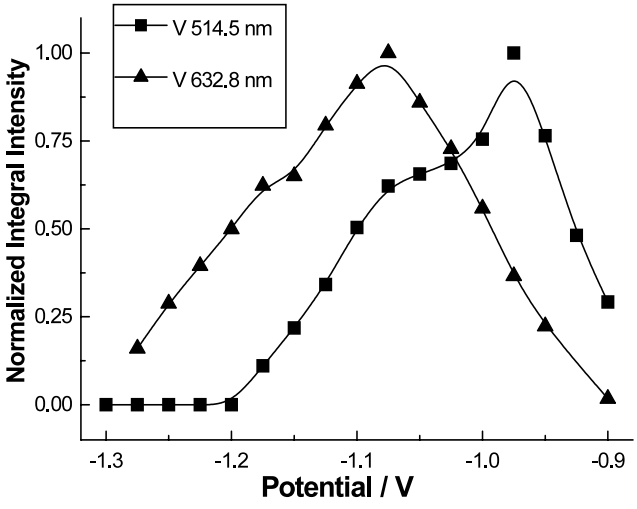

Fig. 6. The profile of the normalized integral intensity of the ring-breathing vibration band of pyridine as the function of the potential on Co surfaces in 10^{-2} M pyridine+0.1 M $NaClO_4$.

potential should move to a more negative potential, in order to match the energy of charge transfer with the incident laser energy. This characteristic reveals that the photon-driven charge (electron) transfer is initiated from the metal to pyridine [59].

It is of special interest that the curve shape of the potential-dependent profile shown in Fig. 6 is very asymmetric, differing remarkably from that of the Py/Ag system [59]. With the negative shift of potential, the intensity of the ν_1 mode increases quickly first, then decreases slowly with a shoulder peak in the profile. By curve iteration, we obtain two peaks; the position of each peak also changes with a change in exciting line, showing a negative shift about 100 mV for a change from 514.5 to 632.8 nm. Fig. 7 gives the schematic diagram of the photo-driven CT model for the Py/Co system, which has two excited states. There are two LUMOs ($3b_1$, $2a_2$) with different energies for the pyridine molecular orbital, which allows two ways for the charge transfer from cobalt to pyridine to occur. From the theoretical calculation, these two peaks can probably be attributed to the formation of two excited CT states, which very likely arise from the excitation of the 4s orbital to the mixing orbital of the metal $4p_x$ and π-typical $3b_1$ of pyridine (CT1), and the excitation of the 3d orbital to the π-typical $2a_2$ orbital of pyridine (CT2), respectively [46,60,61].

Under the assumption of the EM EF being independent of the electrode potential, the change of intensity-potential profiles with different excitation lines is considered mainly from the chemical enhancement viewpoint. On the basis of the Fermi golden rule, we can analyze the contribution from the coupling effect between the CT state and the ring-breathing mode to the

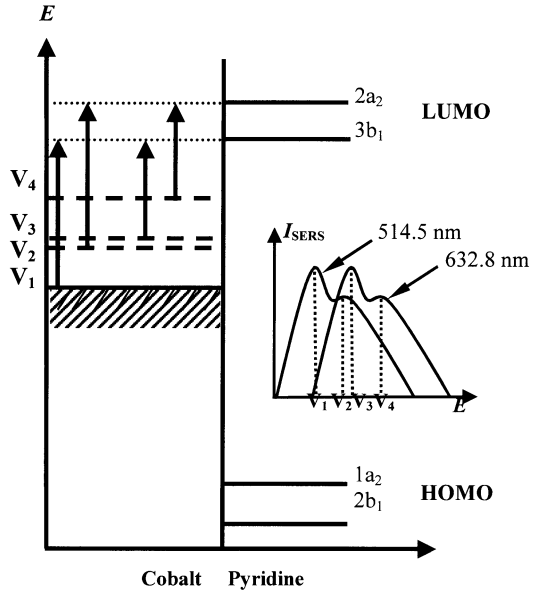

Fig. 7. Schematic diagram of the photo-driven CT model of pyridine adsorbed at a cobalt surface. Charge transfer from metal to pyridine.

total SERS intensity by the formula as [62]

$$I = \frac{8\pi}{9\hbar^2 c^4}\omega_s^3\omega_i(EF)\sum_{\rho}|\alpha_{\rho\rho}|^2 \tag{4}$$

where ω_i and ω_s are the frequencies of the incident and Raman scattering radiations. The subscript $\rho\rho$ of the polarizability tensor $\alpha_{\rho\rho}$ is one of xx, yy, or zz for the a_1 symmetric mode. The Raman polarizability tensors can be expressed by

$$\alpha_{\rho\rho} = \sum_k \frac{M_\rho^2\langle f|k\rangle\langle k|i\rangle}{E_0 + \varepsilon_k - \varepsilon_i - \hbar\omega_i - i\Gamma} \tag{5}$$

in the expression M_ρ is the transition dipole moment along the ρ direction. E_0 is the energy difference between the intermediate and the initial states, where the energy position of the latter state varies with the applied potential. [63,64] $|i\rangle$, $|k\rangle$ and $|f\rangle$ are vibrational wavefunctions; ε_i and ε_k are the vibrational energies at the electronic ground and excited states, respectively. Γ is the damping constant of the excited charge transfer states. In this case, the Raman Franck-Condon integral of the fundamental of the ring-breathing mode is given by [62]

$$\langle 1|k\rangle\langle k|0\rangle = \left(\frac{\Delta^{2k}}{2^k\sqrt{2k!}}\right)\left(\Delta - \frac{2k}{\Delta}\right)\exp\left(-\frac{\Delta^2}{2}\right) \tag{6}$$

where k denotes the vibrational level at the CT states. For both excited CT states, we obtain the dimensionless displacements of the ring-breathing mode by the expressions [65]

$$\Delta = \left(\frac{4\pi^2 c}{h}\right)^{1/2}\left(\frac{\nu^{CT}\nu^G}{\nu^{CT} + \nu^G}\right)^{1/2}(\Delta Q) \tag{7}$$

$$(\Delta Q) = \mu^{1/2}(\Delta R) \tag{8}$$

$$(\Delta R) = \frac{2}{\sqrt{6}}[(\Delta R_{C-N}) + (\Delta R_{C-C}) + (\Delta R'_{C-C})] \tag{9}$$

where h and c are Planck's constant and the light speed. ν_G and ν_{CT} are the vibrational frequencies of the vibrational mode at the ground and excited CT states, respectively. ΔR_{C-N}, ΔR_{C-C}, and $\Delta R'_{C-C}$ are the changes of the C–N and C–C bond distances at the CT states with respect to the geometry of the ground state. By using the B3LYP/6-31+G** method and Eqs. (7)–(9), the values of Δ are determined to be 0.625 and 0.654 for the CT1 and CT2 states, respectively. Considering the vibrational level up to 3, we have a fitting of the Eq. (4) to the experimental data shown in Fig. 6 to obtain the contribution of both CT states in the intensity-potential profiles. We can calculate that the total contributions from both excited CT states are 34.77 and 22.95 $Å^6$ at −0.98 and −1.08 V (the peak positions in Fig. 6), respectively, at the excitation wavelength of 514.5 nm. On the other hand, for the excitation wavelength of

632.8 nm, the squares of the resonance Raman polarizabilities are 19.19 and 11.76 Å^6 at −1.08 and −1.18 V.

The chemical EF can be estimated by the ratio of the resonance Raman scattering intensity arising from both the CT states of pyridine adsorbed on the surface and the normal Raman scattering intensity of the free pyridine molecule. Thus, the chemical enhancement can be written by [66]

$$f_{CE} = \frac{\sum_{n=1}^{n}\sum_{\rho}|\alpha_{\rho\rho,n}|^2}{b^2(v_i+1)\left(\frac{\partial\alpha}{\partial Q}\right)^2} \quad (10)$$

where

$$b^2 = \frac{h}{8\pi^2\omega} \quad (11)$$

is the zero point amplitude of the ring-breathing mode here. The derivative of the polarizability along the ring-breathing normal mode is predicted as about 24.36 Å^4 amu^{-1} by means of density functional calculation (B3LYP/6-31+G**/LanL2DZ). Since only the fundamental frequency is considered here, $v_i = 1$ and then $2b^2 = 0.0334$ Å^2 amu. Thus, we can obtain the denominator of 0.81 Å^6 in the above equation. Hence, the EFs for the exciting line of 514.5 nm are 43- and 28-fold for the above two potentials, respectively. For the exciting line of 632.8 nm, the EFs are about 24- and 15-fold at −1.08 and −1.18 V, respectively. Accordingly, one can propose that there is about a one order of magnitude difference from the charge transfer enhancement for pyridine adsorbed at the cobalt surface.

It should be pointed out that, regarding the use of the EM or CT mechanism, it is still difficult to explain the SERS spectral features, such as the potential-dependent relative intensity as mentioned above. For example, the band intensity of v_{12} (1032 cm^{-1}) of pyridine was too weak to be detected in the present study, though it is almost as strong as the v_1 (1004 cm^{-1}) mode in the normal Raman spectrum of liquid pyridine. This mode presents quite a high intensity in the SERS spectra on silver in a wide potential range [11]. Since both v_1 and v_{12} modes belong to the a_1 mode, it is hard to explain the vanishing of the v_{12} band of the Py/Co system only with the difference of adsorption mode or SERS contribution to different modes. Therefore, a preferable explanation may be related to the interaction between adsorbed pyridine with the substrate.

Through the quantum chemical calculation on the pyridine–metal complexes, we found that the chemical interaction between pyridine and the metal leads to a change of the Raman intensities of different a_1 modes to different extents. In particular, our result shows that the significant changes in the relative Raman intensities of the v_{12} mode of pyridine–metal complexes are due mainly to the fact that the Raman scattering cross-section of this vibrational mode is very sensitive to two factors: (i) the chemical interaction between metal and pyridine and (ii) the CT mechanism [67]. In the case where factor (ii) was present, the relative intensity of the v_{12} mode always decreases to some extent for pyridine interaction with the metal. However, factor (i) plays the more important role when the chemical interaction is strong. The calculation infers a stronger interaction of pyridine with cobalt than that with silver. Due to the weak bonding between pyridine and silver, the interaction does not greatly influence the relative intensities of bands of v_1 and v_{12} modes. On the other hand, the intensity of the v_{12} band is weakened significantly due to the strong bonding between pyridine and cobalt.

4. Conclusion

In summary, using an appropriate surface-roughening procedure for Co electrodes and a highly sensitive confocal microprobe Raman system, we have been able to obtain good-quality SERS spectra of pyridine adsorbed at massive Co electrodes over a wide potential range. The remarkable difference in the SERS spectra of pyridine adsorbed on Co and Ag can be explained by the stronger chemical interaction between pyridine and the Co than that with Ag. The SERS generated from the cobalt surface result from joint contributions from the EM field and the CT enhancement. Although the theoretical calculation agrees well with the experimental data, the model of a single nano-spheroid may still be too simple. Recent advances in theory can evaluate the optical response of particles with various shapes for an arbitrarily rough surface of the noble metals [68–70]. The discrete dipole approximation (DDA) is a powerful method [71,72]. However, at the present stage, DDA has not been applied to transition metal systems since their refractive indices are slightly large. It is therefore a challenge to extend this method further to study transition metal systems. Nevertheless, our preliminary experimental and theoretical results have shown that SERS could be developed into a valuable surface diagnostic in situ probe to investigate adsorbate–metal interaction and transition metal | liquid interfaces.

Acknowledgements

The authors gratefully acknowledge the financial support from the Natural Science Foundation of China under contract Nos. 20003008, 20021002 and 90206039.

References

[1] N. Maki, N. Tanaka, in: A.J. Bard (Ed.), Encyclopedia of the Electrochemistry of the Elements, vol. III, Marcel Dekker, New York, 1973, p. 43.
[2] M.B. Davis, Coord. Chem. Rev. 169 (1998) 237.
[3] S.T. Kuk, Y.S. Song, S. Suh, J.Y. Kim, K. Kim, J. Mater. Chem. 11 (2001) 630.
[4] C. Gao, Mater. Res. Innov. 1 (1998) 238.
[5] V. Brusic, G.S. Frankel, A.G. Schrott, T.A. Petersen, B.M. Rush, J. Electrochem. Soc. 140 (1993) 2507.
[6] M. Sawada, H. Hayashi, A. Kakizaki, Phys. Rev. B 63 (2001) 195407.
[7] R. Mamy, Surf. Sci. 322 (1995) 337.
[8] K.M. Ismail, W.A. Badawy, J. Appl. Electrochem. 30 (2000) 1303.
[9] N.J. Cantini, D.B. Mitton, N. Eliaz, G. Leisk, S.L. Wallace, F. Bellucci, G.E. Thompson, R.M. Latanision, Electrochem. Solid State Lett. 3 (2000) 275.
[10] J.M. Nan, Y. Yang, J.K. You, Z.G. Lin, Chem. J. Chin. Univ. 20 (1999) 1276.
[11] M. Fleischmann, P.J. Hendra, A.J. McQuillan, Chem. Phys. Lett. 26 (1974) 163.
[12] D.J. Jeanmaire, R.P. Van Duyne, J. Electroanal. Chem. 84 (1977) 1.
[13] M.G. Albrecht, J.A. Creighton, J. Am. Chem. Soc. 99 (1977) 5215.
[14] R.K. Chang, T.E. Furtak, Surface Enhanced Raman Scattering, Plenum Press, New York, 1982.
[15] A. Otto, in: M. Cardona, G. Guntherodt (Eds.), Light Scattering in Solid, vol. IV, Springer, Berlin, 1984, p. 289.
[16] M. Moskovits, Rev. Mod. Phys. 57 (1985) 783.
[17] M. Fleischmann, I.R. Hill, in: R.E. White, J.O'M. Bockris, B.E. Conway, E. Yeager (Eds.), Comprehensive Treatise of Electrochemistry, vol. VIII, Plenum Press, New York, 1984, p. 373.
[18] M.J. Weaver, S.Z. Zou, in: A. Wieckowski (Ed.), Interfacial Electrochemistry, Marcel Dekker, New York, 1999, p. 301.
[19] K. Kneipp, H. Kneipp, I. Itzkan, R.R. Dasari, M.S. Feld, Chem. Rev. 99 (1999) 2957.
[20] R.P. Cooney, M. Fleischmann, P.J. Hendra, J. Chem. Soc. Chem. Commun. (1977) 235.
[21] R.P. Cooney, P.J. Hendra, M. Fleischmann, J. Raman Spectrosc. 6 (1977) 264.
[22] B. Pettinger, U. Tiedemann, J. Electroanal. Chem. 228 (1987) 219.
[23] H. Yamada, Y. Yamamoto, Chem. Phys. Lett. 77 (1981) 520.
[24] L.W.H. Leung, M.J. Weaver, J. Electroanal. Chem. 217 (1987) 367.
[25] M. Fleischmann, Z.Q. Tian, L.J. Li, J. Electroanal. Chem. 217 (1987) 397.
[26] M. Fleischmann, Z.Q. Tian, J. Electroanal. Chem. 217 (1987) 411.
[27] S.Z. Zou, C.T. Williams, E.K.Y. Chen, M.J. Weaver, J. Am. Chem. Soc. 120 (1998) 3811.
[28] S.A. Bilmes, J.C. Rubim, A. Otto, J.C. Arvia, Chem. Phys. Lett. 159 (1989) 89.
[29] S.A. Bilmes, Chem. Phys. Lett. 171 (1990) 141.
[30] G. Mengoli, M.M. Musiani, M. Fleischmann, B.W. Mao, Z.Q. Tian, Electrochim. Acta 32 (1987) 1239.
[31] S.Z. Zou, M.J. Weaver, X.Q. Li, B. Ren, Z.Q. Tian, J. Phys. Chem. B 103 (1999) 4218.
[32] S.Z. Zou, M.J. Weaver, Anal. Chem. 70 (1998) 2387.
[33] M.J. Weaver, S.Z. Zou, H.Y.H. Chan, Anal. Chem. 72 (2000) 38A.
[34] M.F. Mrozek, H. Luo, M.J. Weaver, Langmuir 16 (2000) 8463.
[35] M.F. Mrozek, Y. Xie, M.J. Weaver, Anal. Chem. 73 (2001) 5953.
[36] S.Z. Zou, M.J. Weaver, J. Phys. Chem. B 103 (1999) 2323.
[37] C.J. Zhong, Z.Q. Tian, Z.W. Tian, Sci. China B (1990) 1233.
[38] B. Ren, Q.J. Huang, W.B. Cai, B.W. Mao, F.M. Liu, Z.Q. Tian, J. Electroanal. Chem. 415 (1996) 175.
[39] Z.Q. Tian, B. Ren, B.W. Mao, J. Phys. Chem. B 101 (1997) 1338.
[40] Z.Q. Tian, J.S. Gao, X.Q. Li, B. Ren, Q.J. Huang, W.B. Cai, F.M. Liu, B.W. Mao, J. Raman Spectrosc. 29 (1998) 703.
[41] W.B. Cai, B. Ren, X.Q. Li, C.X. She, F.M. Liu, X.W. Cai, Z.Q. Tian, Surf. Sci. 406 (1998) 9.
[42] P.G. Cao, J.L. Yao, B. Ren, B.W. Mao, R.A. Gu, Z.Q. Tian, Chem. Phys. Lett. 316 (2000) 1.
[43] B. Ren, X.F. Lin, J.W. Yan, B.W. Mao, Z.Q. Tian, J. Phys. Chem. B 107 (2003) 899.
[44] Z.Q. Tian, B. Ren, in: A.J. Bard, M. Stratmann (Eds.), Encyclopedia of Electrochemistry, vol. III, Wiley/VCH, New York, 2003, p. 572.
[45] D.Y. Wu, Y. Xie, B. Ren, J.W. Yan, B.W. Mao, Z.Q. Tian, Phys. Chem. Commun. (2001) 18.
[46] Z.Q. Tian, B. Ren, D.Y. Wu, J. Phys. Chem. B 106 (2002) 9463.
[47] J. Gersten, A. Nitzan, J. Chem. Phys. 73 (1980) 3023.
[48] S.H. Macomber, T.E. Furtak, Chem. Phys. Lett. 90 (1982) 59.
[49] J.R. Lombardi, B. Davis, Chem. Rev. 102 (2002) 2431.
[50] F.J. Adrian, Chem. Phys. Lett. 78 (1981) 45.
[51] M. Kerker, Acc. Chem. Res. 17 (1984) 271.
[52] M. Kerker, S. Wang, H. Chew, Appl. Opt. 19 (1980) 4159.
[53] M.P. Cline, P.W. Barber, R.K. Chang, J. Opt. Soc. Am. B 3 (1986) 15.
[54] B.J. Messinger, K. Ulrich Von Raben, R.K. Chang, P.W. Barber, Phys. Rev. B 24 (1981) 649.
[55] J.L. Yao, J. Tang, D.Y. Wu, D.M. Sun, K.H. Xue, B. Ren, B.W. Mao, Z.Q. Tian, Surf. Sci. 514 (2002) 108.
[56] R.L. Birke, J.R. Lombardi, in: R.J. Gale (Ed.), Spectroelectrochemistry—Theory and Practice, Plenum, New York, 1988, p. 263.
[57] A. Campion, P. Kambhampati, Chem. Soc. Rev. 27 (1998) 241.
[58] D.A. Guzonas, D.E. Irish, G.F. Atkinson, Langmuir 6 (1990) 1102.
[59] M.A. Bryant, S.L. Loa, J.E. Pemberton, Langmuir 8 (1992) 753.
[60] J.A. Creighton, in: Z.Q. Tian, B. Ren (Eds.), Progress in Surface Raman Spectroscopy, Xiamen University Press, Xiamen, China, 2000, p. 11.
[61] R. Bauernschmitt, R. Ahrichs, Chem. Phys. Lett. 256 (1996) 454.
[62] A.M. Michaels, J. Jiang, L. Brus, J. Phys. Chem. B 104 (2000) 11965.
[63] A. Kudelski, J. Bukowska, Chem. Phys. Lett. 222 (1994) 555.
[64] J.C. Rubim, P. Corio, M.C.C. Ribeiro, M. Matz, J. Phys. Chem. 99 (1995) 15765.
[65] R.J.H. Clark, T.J. Dines, Angew. Chem. Int. Ed. Engl. 25 (1986) 31.
[66] B.S. Galabov, T. Dudev, Vibrational Intensities, Elsevier, Amsterdam, 1996.
[67] D.Y. Wu, M. Hayashi, S.H. Lin, Z.Q. Tian, Spectrochim. Acta A, in press.
[68] T.R. Jensen, G.C. Schatz, R.P. Van Duyne, J. Phys. Chem. 103 (1999) 2394.
[69] G.C. Schatz, J. Mol. Struct. (THEOCHEM) 573 (2001) 73.
[70] G.C. Schatz, R.P. Van Duyne, in: J.M. Chalmers, P.R. Griffiths (Eds.), Handbook of Vibrational Spectroscopy, Wiley, Chichester, 2002.
[71] B.T. Draine, P.J. Flatan, J. Opt. Soc. Am. A 11 (1994) 1491.
[72] B.T. Draine, P.J. Flatan, User's Guide to the discrete Dipole Approximation code DDSCAT, version 5a10, 2000. Available from http://xxx.lanl.gov/abs/astro-ph/0008151v2.